The Journal of Chemical Physics

RESEARCH ARTICLE | JUNE 27 2022

Breaking covalent bonds in the context of the many-body expansion (MBE). I. The purported "first row anomaly" in XH_n (X = C, Si, Ge, Sn; n = 1–4)

Demeter Tzeli ; Sotiris S. Xantheas

J. Chem. Phys. 156, 244303 (2022)
https://doi.org/10.1063/5.0095329

The Journal of Chemical Physics ARTICLE scitation.org/journal/jcp

Breaking covalent bonds in the context of the many-body expansion (MBE). I. The purported "first row anomaly" in XH_n (X = C, Si, Ge, Sn; n = 1–4)

Cite as: J. Chem. Phys. 156, 244303 (2022); doi: 10.1063/5.0095329
Submitted: 9 April 2022 • Accepted: 22 May 2022 •
Published Online: 27 June 2022 • Publisher Error Corrected: 01 September 2022

Demeter Tzeli[1,2] and Sotiris S. Xantheas[3,4,a)]

AFFILIATIONS

[1] Laboratory of Physical Chemistry, Department of Chemistry, National and Kapodistrian University of Athens, Panepistimiopolis Zografou, Athens 15784, Greece
[2] Theoretical and Physical Chemistry Institute, National Hellenic Research Foundation, 48 Vassileos Constantinou Avenue, Athens 11635, Greece
[3] Advanced Computing, Mathematics and Data Division, Pacific Northwest National Laboratory, 902 Battelle Boulevard, P.O. Box 999, MS K1-83, Richland, Washington 99352, USA
[4] Department of Chemistry, University of Washington, Seattle, Washington 98195, USA

Note: This paper is part of the JCP Special Topic on Nature of the Chemical Bond.
[a)] **Authors to whom correspondence should be addressed:** sotiris.xantheas@pnnl.gov and xantheas@uw.edu

ABSTRACT

We present a new, novel implementation of the Many-Body Expansion (MBE) to account for the breaking of covalent bonds, thus extending the range of applications from its previous popular usage in the breaking of hydrogen bonds in clusters to molecules. A central concept of the new implementation is the *in situ* atomic electronic state of an atom in a molecule that casts the one-body term as the energy required to promote it to that state from its ground state. The rest of the terms correspond to the individual diatomic, triatomic, etc., fragments. Its application to the atomization energies of the XH_n series, X = C, Si, Ge, Sn and n = 1–4, suggests that the (negative, stabilizing) 2-B is by far the largest term in the MBE with the higher order terms oscillating between positive and negative values and decreasing dramatically in size with increasing rank of the expansion. The analysis offers an alternative explanation for the purported "first row anomaly" in the incremental $H_{n-1}X$–H bond energies seen when these energies are evaluated with respect to the lowest energy among the states of the XH_n molecules. Due to the "flipping" of the ground/first excited state between CH_2 ($^3B_1$ ground state, $^1A_1$ first excited state) and XH_2, X = Si, Ge, Sn ($^1A_1$ ground state, $^3B_1$ first excited state), the overall picture does not exhibit a "first row anomaly" when the incremental bond energies are evaluated with respect to the molecular states having the same *in situ* atomic states.

I. INTRODUCTION

The Many-Body Expansion (MBE) is a concept based on combinatorial mathematics that was first introduced over 300 years ago and is usually employed to count the number of elements in the union of finite sets.[1] Its first application to chemical physics problems considered individual water molecules as "bodies" connected via hydrogen bonds as it was used to estimate the non-additive three-body term by partitioning the energy of a water trimer.[2] Since then the MBE analysis based on the energies of distinct, non-overlapping sub-fragments has been applied to hydrogen bonded clusters by some of us[3–9] and others[10–27] to quantify the importance of non-additive terms in the binding energies of aqueous clusters. Recently, the details of the MBE based on high level electronic structure calculations related to the size of the orbital basis set and the level of electron correlation used in the expansion[28–30] as well as a molecular dynamics protocol based on the MBE (MBE-MD)[31] were reported. This type of MBE for hydrogen bonded

molecular systems (including ions), where the definition of a "body" is straightforward and the system is partitioned in non-overlapping sub-fragments (monomers, dimers, trimers, etc.) by just breaking hydrogen bonds, has laid the foundation for the development of accurate, *ab initio* based, many-body interaction potentials for water.[32–53] This is to be contrasted to different partitions that are, for instance, based on overlapping sub-fragments, such as the Molecular Tailoring Approach (MTA),[54–59] or other fragmentation based approaches.[60–64] Note that the MBE has also been applied to incorporate molecular orbitals as "bodies" in order to extrapolate the total correlation energy of molecules[65–72] and solids.[73–75]

In this paper, we extend the general idea of the MBE to the breaking of covalent bonds, that is, considering a polyatomic molecule as consisting of a collection of atoms, diatomics, triatomics, etc. A recent study[76] of the carbon, silicon, and germanium hydrides, XH_n (n = 1–4) based on the spin-coupled generalized valence bond theory has examined the qualitative changes between carbon and silicon/germanium in the $H_{n-1}X$–H bond energies (D_e) on the context of the "first raw anomaly"[77] by expanding on Kutzelnigg's argument[78] based on the hybridization of the X atom bond orbitals due to the increase in the spatial separation of the *ns* and *np* orbitals between atoms in the first row and the following rows of the Periodic Table. The results presented in our study offer (*vide infra*) an alternative explanation for this result.

Our analysis is based on casting the atomization energy ($\Delta E_{atomiz.}$) of a molecule of N atoms computed with respect to its constituent atoms i (i = 1, . . ., N) in their respective ground states (E_i^0) in the usual way[4] as

$$\Delta E_{atomiz.} = \Delta E(1-B) + \Delta E(2-B) + \Delta E(3-B) + \cdots + \Delta E(n-B), \quad (1)$$

where

$$\Delta E(1-B) = \sum_i^N \left(E_i^p - E_i^0\right), \quad (2)$$

$$\Delta E(2-B) = \sum_{i,j}^N \Delta^2 E_{ij} = \sum_{i,j}^N (E_{ij}^{pq} - E_i^p - E_j^q), \quad (3)$$

$$\Delta E(3-B) = \sum_{i,j,k}^N \Delta^3 E_{ijk} = \sum_{i,j,k}^N \left(E_{ijk}^{pqr} - \Delta^2 E_{ij} - \Delta^2 E_{ik} - \Delta^2 E_{jk} - E_i^p - E_j^q - E_k^r\right), \quad (4)$$

and E_i^p, E_{ij}^{pq}, E_{ijk}^{pqr}, E_{ijkl}^{pqrs}, etc., are the energies of the *in situ* (ground or excited) states of atom (*i*), dimer (*ij*), trimer (*ijk*), tetramer (*ijkl*), etc., in the molecule. It is obvious that if the *in situ* state of an atom in the molecule (E_i^p) is the atom's ground state (E_i^0), the 1-B term for that atom, given by Eq. (2), is zero.

Since the concept of the *in situ* state of an atom in the molecule is central to our analysis, we will further discuss it using Fig. 1, as discussed by Heitler.[79] Consider a carbon atom in its ground (^{3}P) atomic state. The pairing of the four ($2s^2 2p^2$) valence electrons in this electronic state is not appropriate to accommodate bonding with four hydrogen atoms to form CH_4. They should rather be promoted to the ^{5}S excited electronic state lying 4.18 eV above[80] the ^{3}P ground state in order to form the 4 equivalent C–H bonds. In order words, the 2*s* and the three 2*p* orbitals of the carbon atom should be hybridized into four equivalent sp^3 orbitals forming the atomic ^{5}S state, which is the *in situ* electronic state of the carbon atom in CH_4. Examples of the concept of *in situ* atomic states have been previously discussed for molecules[81,82] and metal aqueous clusters.[83,84] As it is evident from Eqs. (1)–(4), the choice of the *in situ* electronic state of an atom will affect the MBE.

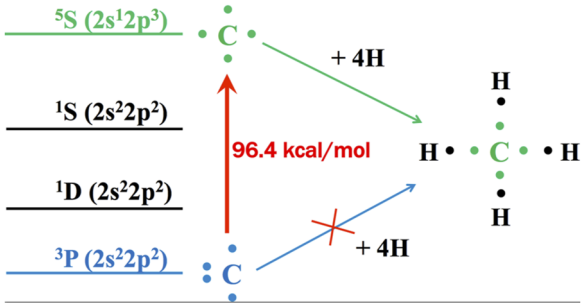

FIG. 1. The *in situ* electronic structure of the carbon atom in CH_4.

II. METHODOLOGY

The calculations for the ground states of the XH_n hydrides, X = C, Si, Ge, Sn and n = 1–4, were performed at the Coupled Cluster Singles, Doubles and perturbative Triples [CCSD(T) and RCCSD(T)][85,86] levels of theory. Additionally, two excited states for CH and one for the remaining diatomic and all triatomic molecules were computed. For the CH_n series, we employed Dunning's augmented correlation consistent basis sets, aug-cc-pV*x*Z, x = D, T, Q.[87,88] For the SiH_n, GeH_n, and SnH_n species, we employed the aug-cc-pVQZ basis sets for H,[87,88] Si,[89] and Ge,[90] and for Sn Peterson's[91] aug-cc-pVQZ-PP augmented correlation consistent basis sets, which employ accurate small-core ($1s^2 2s^2 2p^6 3s^2 3p^6 3d^{10}$; 28 electrons) relativistic pseudopotentials.

The atomization energies, the XH_{n-1}–H dissociation energies, and the individual many body terms were corrected for basis set superposition error (BSSE)[92,93] as described in Ref. 94. Note that the deformation (or relaxation) energy in that reference that arises from geometrical distortions due to the interaction is zero in the present case since the atomization energy is computed with respect to the atoms. The BSSE-corrected interaction energies ($\Delta E'_{atomiz.}$) and the BSSE-corrected many-body terms, $\Delta E'(n\text{-B})$, e given in Eqs. (5)–(10),[4]

$$\Delta E'_{atomiz.} = E^{X_i X_j \cdots}_{X_i X_j \ldots}(X_i X_j \cdots) - \sum_i E^{X_i X_j \cdots}_{X_i X_j \ldots}(X_i), \quad (5)$$

$$\Delta E'(1-B) = \Delta E(1-B), \quad (6)$$

$$\Delta E'(2-B) = \sum_{i,j} \Delta^2 E'_{ij}, \quad (7)$$

$$\Delta^2 E'_{ij} = E^{X_1X_2\cdots}_{X_1X_2\ldots}(X_iX_j) - \left\{E^{X_1X_2\cdots}_{X_1X_2\ldots}(X_i) + E^{X_1X_2\cdots}_{X_1X_2\ldots}(X_j)\right\}, \quad (8)$$

$$\Delta E'(3-B) = \sum_{i,j,k} \Delta^3 E'_{ijk}, \quad (9)$$

$$\begin{aligned}\Delta^3 E'_{ijk} = {} & E^{X_1X_2\cdots}_{X_1X_2\ldots}(X_iX_jX_k) - \left\{E^{X_1X_2\cdots}_{X_1X_2\ldots}(X_i) + E^{X_1X_2\cdots}_{X_1X_2\ldots}(X_j)\right. \\ & \left. + E^{X_1X_2\cdots}_{X_1X_2\ldots}(X_k)\right\} \\ & - \left\{\Delta^2 E^{X_1X_2\cdots}_{X_1X_2\ldots}(X_iX_j) + \Delta^2 E^{X_1X_2\cdots}_{X_1X_2\ldots}(X_iX_k)\right. \\ & \left. + \Delta^2 E^{X_1X_2\cdots}_{X_1X_2\ldots}(X_jX_k)\right\}, \end{aligned} \quad (10)$$

etc., where $E^s_G(M)$ refers to the total energy of the molecule M computed at the geometry G with basis set s.

In order to evaluate the appropriateness of RCCSD(T), which is a single-reference method, we checked the single (t_1) and the double (t_2) amplitudes[95] as well as the T_1 and D_1 diagnostics.[96,97] For all calculations of the present study, the t_1 and t_2 amplitudes were small and the T_1 and D_1 diagnostics were $T_1 < 0.02$ and $D_1 < 0.04$, expect for the $^4\Sigma^-$ state of XH, for which the diagnostics were $T_1 \sim 0.03$ and $D_1 \sim 0.07$. We can, therefore, conclude that the single reference RCCSD(T) method is an appropriate methodology to be employed for the systems in this study. All calculations were carried out with the MOLPRO suite of codes.[98]

An important detail of the above analysis is that, for each electronic state of the molecule, the two- and higher-body terms are not necessarily computed at the diatomic, triatomic, etc., ground electronic states but at the respective electronic states of these fragments that are formed from the *in situ* electronic states of the constituent atoms in the full molecule. We will further elaborate on this important detail in Sec. III when we present the case of XH_2.

III. RESULTS AND DISCUSSION

A. The MBE for the XH_n series (X = C, Si, Ge, Sn; n = 1–4)

The results in this subsection are presented in Figs. 2–13 and Tables I–V. Below we will discuss the individual members of the XH_n series for each n as well as the trends with the atom identity.

XH (X = C, Si, Ge, Sn): The analysis for the ground ($^2\Pi$), first ($^4\Sigma^-$), and second ($^2\Delta$) excited states of CH is shown in Fig. 2. Energy differences are taken with respect to the ground state of the two atoms, viz., C(^{3}P) + H(^{2}S). The $^2\Pi$ ground state of CH correlates

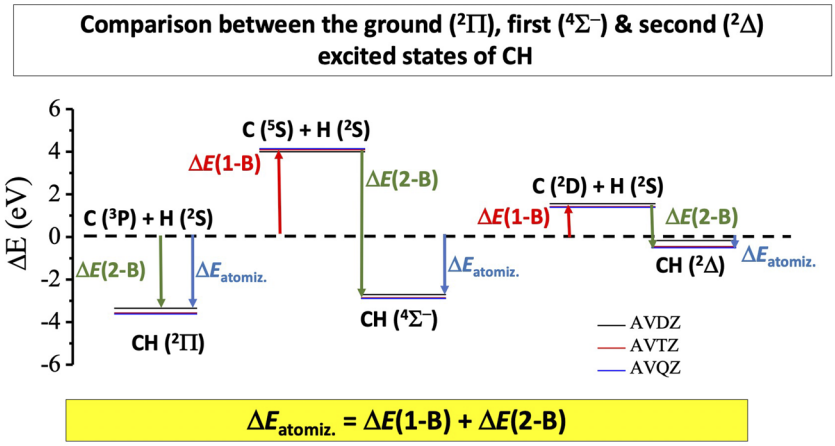

FIG. 2. Many-body decomposition of $\Delta E_{atomiz.}$ for the $^2\Pi$, $^4\Sigma^-$, and $^2\Delta$ states of CH at the RCCSD(T)/aug-cc-pVxZ, x = D, T, Q, level of theory.

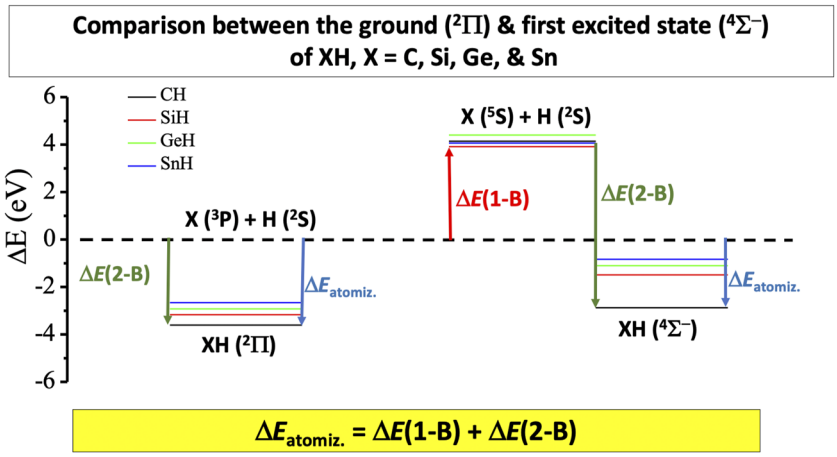

FIG. 3. Many-body decomposition of $\Delta E_{atomiz.}$ for the $^2\Pi$ and $^4\Sigma^-$ states of the XH series (X = C, Si, Ge, Sn) at the RCCSD(T)/aug-cc-pVQZ(-PP)$_{Sn}$ level of theory.

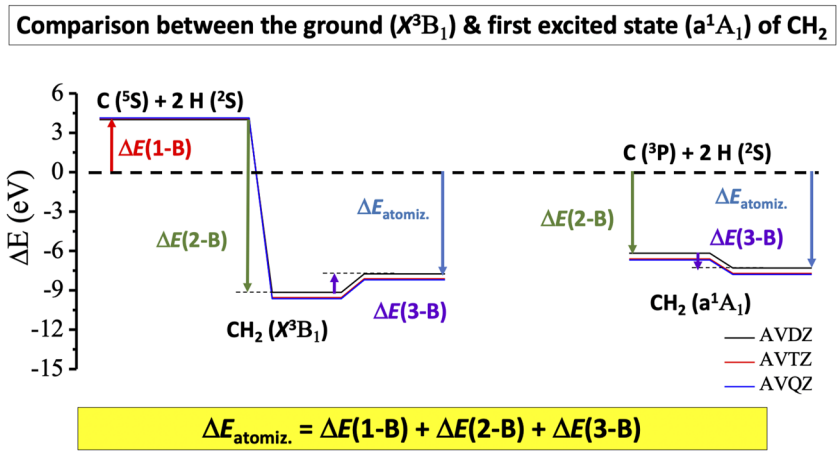

FIG. 4. Many-body decomposition of the $\Delta E_{atomiz.}$ for the X^3B_1 and a^1A_1 states of CH_2 at the RCCSD(T)/aug-cc-pVxZ, x = D, T, Q, level of theory.

with the corresponding ground state atomic states, i.e., the *in situ* atomic state of C in the ground state of CH is the atomic ground ^{3}P state. In other words, the 1-B term is zero since there is no need to promote the ground ^{3}P state of the C atom to form the C–H bond in its ground $^2\Pi$ state. In this case, the 2-B term is identical with the atomization energy ΔE_{atomiz}. However, the situation is different for the first and second excited states of the CH molecule. The *in situ* electronic state of the C atom in the first $^4\Sigma^-$ excited state of CH is the atomic ^{5}S state, so the (positive) 1-B term is the energy required to promote the C atom from ^{3}P → ^{5}S. Accordingly, the

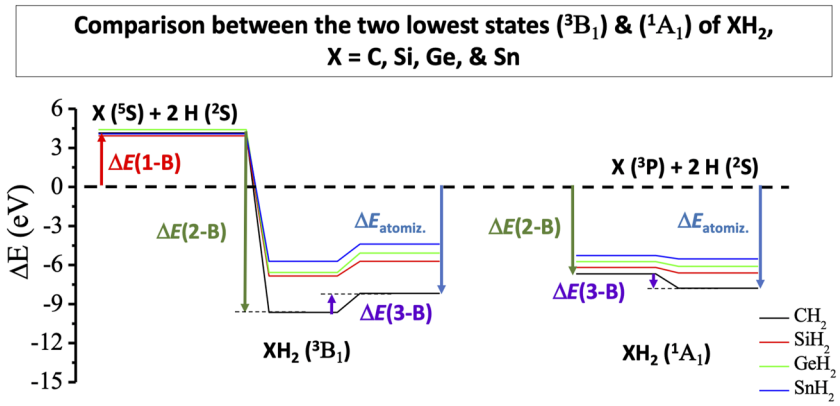

FIG. 5. Many-body decomposition of the $\Delta E_{atomiz.}$ for the $^3B_1$ and $^1A_1$ states of the XH_2 series (X = C, Si, Ge, Sn) at RCCSD(T)/aug-cc-pVQZ(-PP)$_{Sn}$ level of theory.

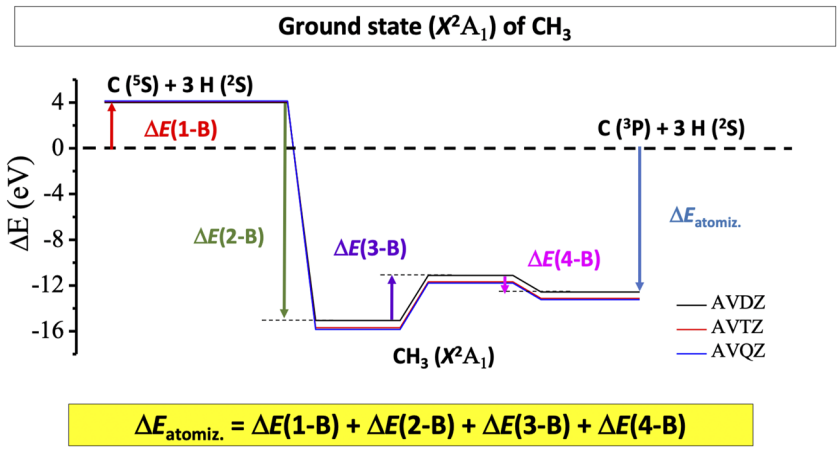

FIG. 6. Many-body decomposition of the $\Delta E_{atomiz.}$ for the X^2A_1 state of CH_3 at the RCCSD(T)/aug-cc-pVxZ, x = D, T, Q, level of theory.

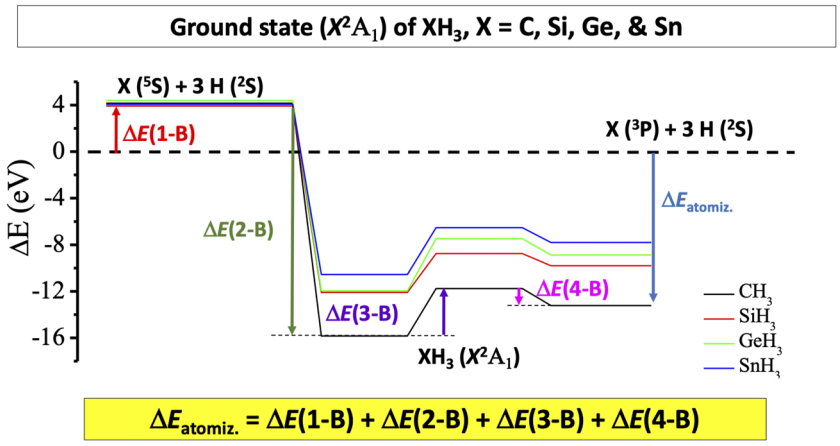

FIG. 7. Many-body decomposition of the $\Delta E_{atomiz.}$ for the X^2A_1 state of the XH_3 series (X = C, Si, Ge, Sn) at the RCCSD(T)/aug-cc-pVQZ(-PP)$_{Sn}$ level of theory.

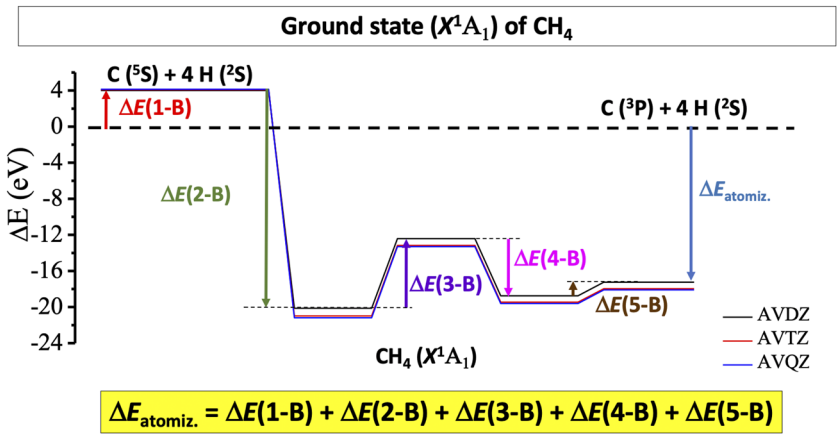

FIG. 8. Many-body decomposition of the $\Delta E_{atomiz.}$ for the X^1A_1 state of CH_4 at the RCCSD(T)/aug-cc-pVxZ, x = D, T, Q, level of theory.

2-B term is the energy difference between the C(^{5}S) + H(^{2}S) and CH($^4\Sigma^-$) energy levels, which is also the difference between the total atomization energy ($\Delta E_{atomiz.}$) and the 1-B term. Similarly, the *in situ* electronic state of the C atom in the second $^2\Delta$ state if CH is the atomic ^{2}D state and the 1-B and 2-B terms are computed accordingly. The results with the various basis sets (AVDZ, AVTZ, and AVQZ) are denoted with different colors for the different energy levels obtained with the three basis sets in Fig. 2. The individual 2-B terms for the ground ($^2\Pi$), first ($^4\Sigma^-$), and second ($^2\Delta$) excited states of CH are decreasing in that order (cf. Table I), and the presence of the repulsive 1-B term for the last two determines the overall order in the atomization energies with respect to the atomic ground

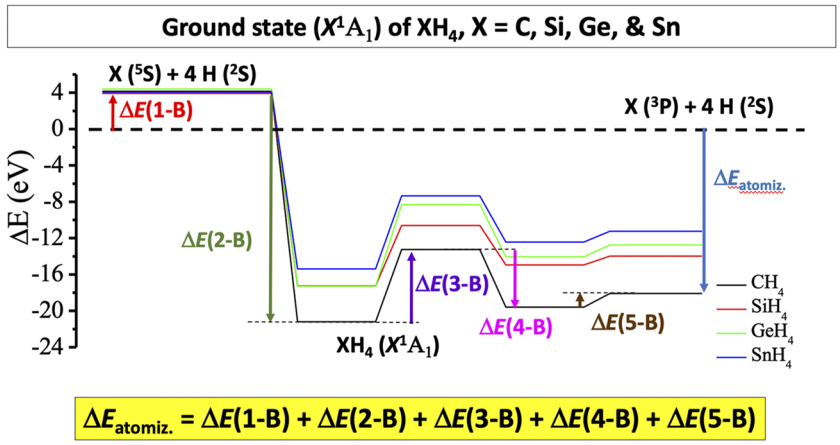

FIG. 9. Many-body decomposition of the $\Delta E_{atomiz.}$ for the X^1A_1 state of the XH_4 series (X = C, Si, Ge, Sn) at the RCCSD(T)/aug-cc-pVQZ(-PP)$_{Sn}$ level of theory.

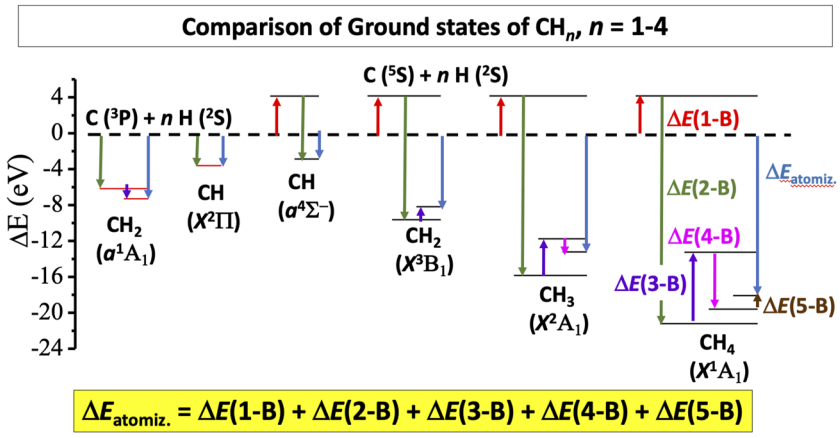

FIG. 10. Summary of the MBE for the $\Delta E_{atomiz.}$ of the CH_n species, n = 1–4, at the RCCSD(T)/aug-cc-pVQZ level of theory.

states, as shown in Fig. 2. The σ bond length of the $^4\Sigma^-$ state is shorter than the corresponding value of the $X^2\Pi$ state by 0.03 Å, showing that the bonding of the $^4\Sigma^-$ state is stronger than in the $X^2\Pi$ state. The 2-B term of the $^4\Sigma^-$ state is significantly larger (double) than the 2-B term of $X^2\Pi$. This happens because the formation of a σ bond with a highly open shell system, such as C(^{5}S), significantly stabilizes the carbon atom and consequently the whole C–H system. On the contrary, the C(^{3}P) is lower in energy than C(^{5}S), it has only two unpaired electrons, and, thus, even though the σ bond stabilize the C–H molecule, this stabilization is not dramatically large.

The situation for the ground ($^2\Pi$) and the first ($^4\Sigma^-$) excited states of SiH, GeH, and SnH is similar to that for CH; the results for the XH series (X = C, Si, Ge, Sn) are graphically summarized in Fig. 3,

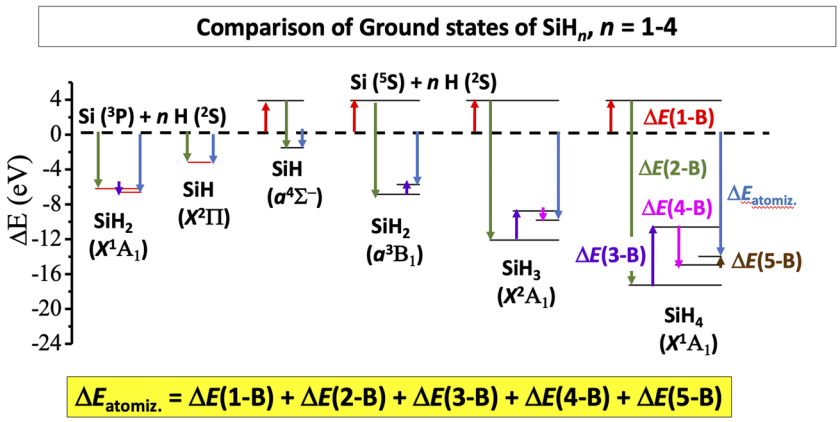

FIG. 11. Many-body decomposition for the $\Delta E_{atomiz.}$ of the SiH_n species, n = 1–4, at RCCSD(T)/aug-cc-pVQZ level of theory.

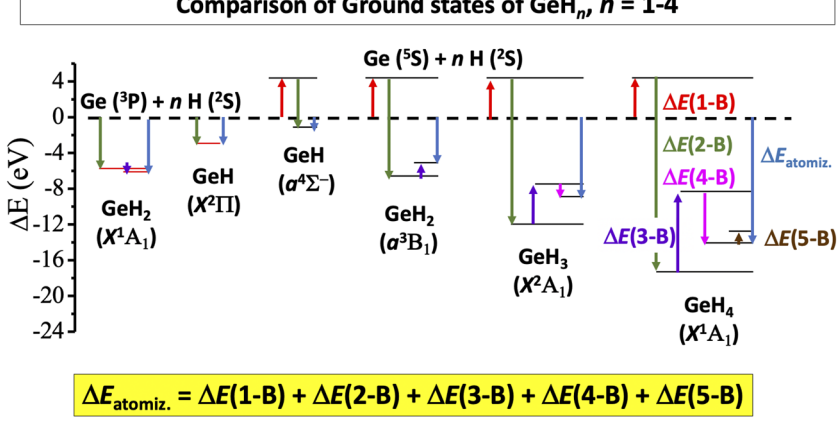

FIG. 12. Many-body decomposition for the $\Delta E_{atomiz.}$ of the GeH_n species, n = 1–4, at RCCSD(T)/aug-cc-pVQZ level of theory.

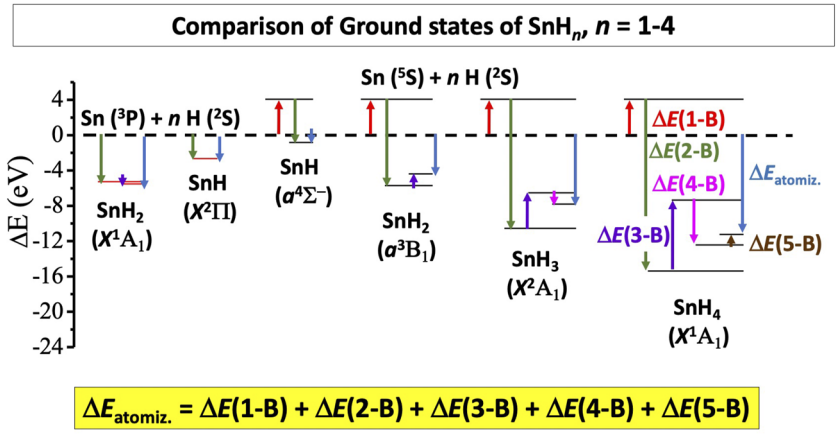

FIG. 13. Many-body decomposition for the $\Delta E_{atomiz.}$ of the SnH_n species, n = 1–4, at RCCSD(T)/aug-cc-pVQZ(-PP)$_{Sn}$ level of theory.

TABLE I. 1-B term (eV), 2-B term (eV), atomization energy $\Delta E_{atomiz.}$ (eV) with respect to ground state products, and dissociation energy ΔE (eV) with respect to the *in situ* atomic state without and with BSSE correction (second lines) of the XH molecules, X = C, Si, Ge, and Sn, at the RCCSD(T) level of theory.

Basis set	Molecule	1-B	2-B	$\Delta E_{atomiz.}$	ΔE
AVDZ	CH ($X^2\Pi$)	0.000	−3.350	−3.350	−3.350
		0.000	−3.309	−3.309	−3.309
	CH ($A^4\Sigma^-$)	4.000	−6.707	−2.707	−6.707
		4.016	−6.679	−2.663	−6.679
	CH ($a^2\Delta$)	1.557	−1.730	−0.173	−1.729
		1.570	−1.713	−0.143	−1.713
AVTZ	CH ($X^2\Pi$)	0.000	−3.571	−3.571	−3.571
		0.000	−3.548	−3.548	−3.548
	CH ($A^4\Sigma^-$)	4.096	−6.960	−2.864	−6.960
		4.111	−6.950	−2.839	−6.950
	CH ($a^2\Delta$)	1.419	−1.871	−0.452	−1.871
		1.430	−1.864	−0.434	−1.864
AVQZ	CH ($X^2\Pi$)	0.000	−3.616	−3.616	−3.616
		0.000	−3.606	−3.606	−3.606
	CH ($A^4\Sigma^-$)	4.139	−7.025	−2.886	−7.025
		4.146	−7.022	−2.876	−7.022
	CH ($a^2\Delta$)	1.391	−1.895	−0.504	−1.895
		1.397	−1.891	−0.494	−1.891
	SiH ($X^2\Pi$)	0.000	−3.172	−3.172	−3.172
		0.000	−3.165	−3.165	−3.165
	SiH ($A^4\Sigma^-$)	3.907	−5.404	−1.497	−5.404
		3.912	−5.402	−1.490	−5.402
	GeH ($X^2\Pi$)	0.000	−2.931	−2.931	−2.931
		0.000	−2.925	−2.925	−2.925
	GeH ($A^4\Sigma^-$)	4.394	−5.505	−1.111	−5.506
		4.398	−5.503	−1.105	−5.504
AVQZ(-PP)$_{Sn}$	SnH ($X^2\Pi$)	0.000	−2.662	−2.662	−2.662
		0.000	−2.658	−2.658	−2.658
	SnH ($A^4\Sigma^-$)	4.061	−4.896	−0.835	−4.896
		4.064	−4.894	−0.830	−4.894

and the individual numbers (including the ones corrected for BSSE) are listed in Table I. The decrease of the individual 2-B terms for the respective ground ($^2\Pi$) and excited ($A^4\Sigma^-$) states in the XH series monotonically follows the trends of increasing X–H separations (cf. Table V) in an almost linear fashion.

XH_2 (X = C, Si, Ge, Sn): The MBE analysis for the ground (X^3B_1) and the first excited (a^1A_1) states of CH_2 is schematically shown in Fig. 4, where the zero in the energy scale is taken with respect to the C(^{3}P) + 2 × H(^{2}S) asymptote. The ground (X^3B_1) state of CH_2 correlates with the C(^{5}S) + H(^{2}S) + H(^{2}S) atomic states so the 1-B term is positive and corresponds to the ^{3}P → ^{5}S promotion energy. The 2-B term is negative, whereas there is a smaller positive 3-B term. The MBE based on the various fragments allows for the further attribution of the individual terms to specific interactions between the constituent atoms. As can be seen from Table II, the main contribution to the total 2-B term (being the sum of the individual interactions between C–H and H–H) comes from the attractive (stabilizing) 2-B_{CH} term with the remaining 2-B_{HH} term being quite small and repulsive (destabilizing), amounting to just ~4% of the total 2-B interaction. In contrast, for the first (a^1A_1) excited state of CH_2, also shown in Fig. 4, the 1-B term is zero (since the *in situ* electronic state of C in the (a^1A_1) state of CH_2 is the atomic ^{3}P state), and, in this case, both the 2- and 3-B terms are negative. This is expected for the 3-B term for the $^1A_1$ state of CH_2 and for the rest of the XH_2 molecules (see below) because this state corresponds to a closed shell system, and, thus, the simultaneous existence of the three atoms further stabilize it. On the contrary, this not the case for the X^3B_1 state in which the system is not closed shell and, thus, it follows the usual trend, i.e., the many-body terms oscillate between the positive and negative values.

The analysis for the combined results for the XH_2 series, X = C, Si, Ge, Sn, are schematically shown in Fig. 5 and listed in Table II. A notable difference between CH_2 and the rest of the XH_2 series (X = Si, Ge, Sn) is that the order of the ground/first excited state is reversed. Indeed, as can be seen from Figs. 4 and 5 and the results of Table I, for CH_2, the ground state is the $^3B_1$ and the first excited the $^1A_1$ state, whereas, for X = Si, Ge, Sn, the ground state of XH_2 is the $^1A_1$ and the first excited the $^3B_1$ state. Therefore, the *in situ*

TABLE II. 1-B term (eV), 2-B term (eV), 3-B term (eV), atomization energy $\Delta E_{\text{atomiz.}}$ (eV) with respect to ground state products, and dissociation energy ΔE (eV) with respect to the *in situ* atomic state without and with BSSE correction (second lines) of the XH_2 molecules, X = C, Si, Ge, and Sn at the RCCSD(T) level of theory. States are listed in decreasing magnitude of ΔE_{atomiz}.

Basis set	Molecule	1-B	2-B_{XH}	2-B_{HH}	2-B	3-B	$\Delta E_{atomiz.}$	ΔE
AVDZ	CH_2 (X^3B_1)	4.000	−6.705	0.259	−13.151	1.404	−7.747	−11.747
		4.031	−6.696	0.249	−13.142	1.449	−7.661	−11.692
	CH_2 (a^1A_1)	0.000	−3.348	0.527	−6.169	−1.127	−7.296	−7.296
		0.000	−3.317	0.516	−6.117	−1.098	−7.214	−7.214
AVTZ	CH_2 (X^3B_1)	4.096	−6.957	0.265	−13.650	1.429	−8.125	−12.221
		4.122	−6.957	0.263	−13.650	1.446	−8.082	−12.204
	CH_2 (a^1A_1)	0.000	−3.570	0.534	−6.605	−1.105	−7.710	−7.710
		0.000	−3.550	0.533	−6.567	−1.101	−7.668	−7.668
AVQZ	CH_2 (X^3B_1)	4.139	−7.023	0.265	−13.780	1.443	−8.198	−12.337
		4.152	−7.024	0.265	−13.782	1.451	−8.180	−12.332
	CH_2 (a^1A_1)	0.000	−3.614	0.534	−6.694	−1.102	−7.795	−7.795
		0.000	−3.606	0.534	−6.678	−1.100	−7.778	−7.778
	SiH_2 (X^1A_1)	0.000	−3.171	0.146	−6.196	−0.425	−6.621	−6.621
		0.000	−3.166	0.146	−6.185	−0.424	−6.609	−6.609
	SiH_2 (a^3B_1)	3.907	−5.403	0.050	−10.755	1.111	−5.737	−9.644
		3.916	−5.403	0.050	−10.756	1.116	−5.725	−9.640
	GeH_2 (X^1A_1)	0.000	−2.930	0.109	−5.752	−0.359	−6.111	−6.111
		0.000	−2.925	0.109	−5.742	−0.358	−6.100	−6.100
	GeH_2 (a^3B_1)	4.394	−5.502	0.034	−10.970	1.481	−5.094	−9.488
		4.402	−5.502	0.033	−10.972	1.487	−5.083	−9.485
AVQZ(-PP)$_{Sn}$	SnH_2 (X^1A_1)	0.000	−2.662	0.049	−5.275	−0.262	−5.537	−5.537
		0.000	−2.658	0.049	−5.267	−0.261	−5.528	−5.528
	SnH_2 (a^3B_1)	4.061	−4.892	0.012	−9.772	1.315	−4.397	−8.457
		4.068	−4.893	0.011	−9.775	1.320	−4.387	−8.455

electronic state of the carbon atom in the ground $^3B_1$ state of CH_2 is C(^{5}S), whereas the *in situ* electronic state of the Si/Ge/Sn in the ground state of $SiH_2/GeH_2/SnH_2$ is Si/Ge/Sn (^{3}P) (see Figs. 4 and 5). The difference on the type of the ground state results from the fact that the Si, Ge, and Sn atoms are larger than C, forming significant larger X–H bond lengths and this favors the formation of two X–H bonds from the X(^{3}P) rather than from the X(^{5}S) states for X = Si, Ge, Sn. Note that the bond arising from the atomic ^{5}S state is stabilized via shorter X–H bond lengths than the one arising from the X(^{3}P) atomic state. Additionally, the 2-B_{XH} and 2-B_{HH} terms are decreasing in the series for both the ground and the excited states, in line with the corresponding monotonic increase of the X–H bond distance (cf. Table V). Note that the 3-B term for the ground (X^3B_1) state is positive (destabilizing), whereas the one for the first excited (a^1A_1) state is negative (stabilizing) in the series. For both states, the 3-B is much smaller than the 2-B term, as seen from Fig. 5 and Table II.

In the following, we elaborate on an important detail of the MBE analysis related to the electronic states used to compute the energies of the fragments. As it can be seen from Figs. 2 and 3, the $^2\Pi$ ground state of XH (X = C, Si, Ge, Sn) is formed from the respective X(^{3}P) + H(^{2}S) states, whereas the first excited ($^4\Sigma^-$) state from the X(^{5}S) + H(^{2}S) states. The ground $^3B_1$ state of CH_2 is formed (cf. Fig. 4) from the C(^{5}S) + 2H(^{2}S) states and, when evaluating the MBE for that state, the two-body "CH" term is computed with CH at its excited $^4\Sigma^-$ state [also formed from C(^{5}S) + H(^{2}S)]. In contrast, the first excited a^1A_1 state of CH_2 is formed (cf. Fig. 4) from C(^{3}P) + 2H(^{2}S) and the two-body "CH" term for that state is computed with CH at its ground $^2\Pi$ state [also formed from C(^{3}P) + H(^{2}S)]. The calculation of the two-body "XH" term in XH_2 for X = Si, Ge, Sn is evaluated in a similar manner while also noting that for these molecules the order of the ground and first excited states flip with respect to CH_2 (see Fig. 5 and Table II). This protocol is also followed in the evaluation of the MBE for the larger molecules.

XH_3 (X = C, Si, Ge, Sn): The MBE for the ground (X^2A_1) state of CH_3 is schematically shown in Fig. 6. The ground state of CH_3 correlates with the C(^{5}S) + H(^{2}S) + H(^{2}S) + H(^{2}S) atomic states, viz., there is a positive 1-B term corresponding to the promotion $^3P \rightarrow {}^5S$ for the carbon atom. The 3-B term is smaller than the 2-B and positive, whereas the 4-B is even smaller than the 3-B and negative. The trends for the MBE of the XH_3 series, X = C, Si, Ge, Sn, schematically shown in Fig. 7 and listed in Table III, are similar to the ones for CH_3 with the terms oscillating between the positive (destabilizing) and negative (stabilizing) values, whereas they overall

TABLE III. 1-B term (eV), 2-B term (eV), 3-B term (eV), 4-B term (eV), atomization energy $\Delta E_{atomiz.}$ (eV) with respect to ground state products, and dissociation energy ΔE (eV) with respect to the *in situ* atomic state without and with BSSE correction (second lines) of the XH_3 molecules, X = C, Si, Ge, and Sn at the RCCSD(T) level of theory.

Basis set	Molecule	1-B	2-B_{XH}	2-B_{HH}	2-B	3-B_{XHH}	3-B_{HHH}	3-B	4-B	$\Delta E_{atomiz.}$	ΔE
AVDZ	CH_3 ($^2A_1$)	4.000	−6.704	0.352	−19.056	1.380	−0.199	3.942	−1.453	−12.567	−16.567
		4.045	−6.715	0.341	−19.120	1.435	−0.197	4.108	−1.475	−12.441	−16.486
AVTZ	CH_3 ($^2A_1$)	4.096	−6.958	0.362	−19.786	1.406	−0.212	4.006	−1.443	−13.128	−17.224
		4.130	−6.965	0.360	−19.814	1.428	−0.212	4.073	−1.460	−13.071	−17.201
AVQZ	CH_3 ($^2A_1$)	4.139	−7.023	0.363	−19.980	1.420	−0.213	4.048	−1.451	−13.244	−17.383
		4.156	−7.027	0.362	−19.995	1.430	−0.213	4.078	−1.459	−13.220	−17.376
	SiH_3 ($^2A_1$)	3.907	−5.402	0.068	−16.003	1.117	−0.028	3.322	−1.052	−9.826	−13.733
		3.918	−5.405	0.068	−16.013	1.124	−0.028	3.343	−1.058	−9.809	−13.727
	GeH_3 ($^2A_1$)	4.394	−5.501	0.049	−16.356	1.495	−0.019	4.467	−1.400	−8.895	−13.289
		4.405	−5.505	0.049	−16.367	1.503	−0.019	4.490	−1.407	−8.879	−13.284
AVQZ(-PP)$_{Sn}$	SnH_3 ($^2A_1$)	4.061	−4.892	0.020	−14.618	1.337	−0.006	4.006	−1.260	−7.811	−11.872
		4.070	−4.896	0.019	−14.629	1.344	−0.006	4.026	−1.266	−7.799	−11.869

decrease in magnitude with rank k after the 2-B term, as can also be seen from Table III. The MBE, therefore, seems to be "converging" albeit in a slow, oscillating manner. Again, the total 2-B_{XH} (sum of three identical components) is the major contributor to the 2-B term with the 2-B_{HH} term being quite small and repulsive as in the XH_2 series; they both decrease in magnitude in the series. With regard to the 3-B term, the signs of the individual components are reversed when compared to the 2-B term: the 3-BX_{HH} is positive, whereas the 3-B_{HHH} is very small and negative.

XH_4 (X = C, Si, Ge, Sn): The *in situ* atomic state of carbon in the ground (X^1A_1) state of CH_4 is ^5S, giving rise to a positive 1-B energy. The negative (stabilizing) 2-B term is the largest one among the higher order terms, which are oscillating between the positive and negative values and are decreasing in size after the 2-B term as can be seen from Fig. 8. The same trends are observed for the rest of the XH_4 series (X = C, Si, Ge, Sn) as shown in Fig. 9 and Table IV. The 3-B_{XHH} and 3-B_{HHH} terms are similar in sign, magnitude, and trend across the XH_4 series as in the XH_3 series. The same behavior is seen for the 4-B_{XHHH} and 4-B_{HHHH} terms (cf. Table IV). A notable difference is that the total (positive) 3-B term almost cancels the total (negative) 4-B term. The 5-B term is small (~10% of the atomization energy).

Trends in the MBE of XH_n (X = C, Si, Ge, Sn): The MBE for the XH_n series is summarized in Figs. 10–13 for X = C, Si, Ge, and Sn, respectively. The trends in both the sign and magnitude of the individual MBE terms are similar across the series, namely, that the 1-B term is zero for n = 1 and positive (energy for the $^3P \rightarrow {}^5S$ promotion of the carbon atom) for n = 2–4 with the 2-B term being

TABLE IV. 1-B term (eV), 2-B term (eV), 3-B term (eV), 4-B term (eV), 5-B term (eV), atomization energy $\Delta E_{atomiz.}$ (eV) with respect to ground state products, and dissociation energy ΔE (eV) with respect to the *in situ* atomic state without and with BSSE correction (second lines) of the XH_4 molecules, X = C, Si, Ge, and Sn at the RCCSD(T) level of theory.

Basis set	Molecule	1-B	2-B_{XH}	2-B_{HH}	2-B	3-B_{XHH}	3-B_{HHH}	3-B	4-B_{XHHH}	4-B_{HHHH}	4-B	5-B	$\Delta E_{atomiz.}$	ΔE
AVDZ	CH_4 ($^1A_1$)	4.000	−6.707	0.451	−24.124	1.463	−0.267	7.711	−1.625	0.157	−6.343	1.511	−17.244	−21.244
		4.036	−6.729	0.439	−24.283	1.522	−0.264	8.074	−1.658	0.160	−6.471	1.537	−17.108	−21.143
AVTZ	CH_4 ($^1A_1$)	4.096	−6.960	0.461	−25.070	1.488	−0.282	7.804	−1.615	0.171	−6.290	1.500	−17.961	−22.057
		4.131	−6.976	0.460	−25.147	1.515	−0.281	7.963	−1.634	0.171	−6.363	1.519	−17.897	−22.028
AVQZ	CH_4 ($^1A_1$)	4.139	−7.025	0.463	−25.322	1.502	−0.284	7.880	−1.620	0.173	−6.307	1.507	−18.104	−22.243
		4.157	−7.033	0.462	−25.357	1.515	−0.284	7.953	−1.630	0.173	−6.346	1.516	−18.078	−22.234
	SiH_4 ($^1A_1$)	3.907	−5.402	0.074	−21.164	1.124	−0.032	6.620	−1.083	0.013	−4.318	0.961	−13.994	−17.901
		3.919	−5.407	0.074	−21.185	1.133	−0.031	6.671	−1.090	0.013	−4.347	0.968	−13.974	−17.893
	GeH_4 ($^1A_1$)	4.394	−5.500	0.054	−21.675	1.503	−0.021	8.933	−1.432	0.008	−5.721	1.311	−12.758	−17.152
		4.406	−5.506	0.054	−21.699	1.512	−0.021	8.989	−1.441	0.008	−5.755	1.319	−12.740	−17.146
AVQZ(-PP)$_{Sn}$	SnH_4 ($^1A_1$)	4.061	−4.890	0.021	−19.434	1.334	−0.007	7.979	−1.260	0.002	−5.039	1.177	−11.255	−15.316
		4.071	−4.895	0.021	−19.456	1.343	−0.007	8.029	−1.268	0.002	−5.069	1.185	−11.240	−15.312

TABLE V. Bond distances R_{XH} (Å) and angles φ_{HXH} (degrees) for the various states of XH_n, (X = C, Si, Ge, Sn; n = 1–4) at the RCCSD(T) level of theory.

		CH_n			SiH_n	GeH_n	SnH_n
		AVDZ	AVTZ	AVQZ	AVQZ	AVQZ	AVQZ
$XH(\chi^2\Pi)$	R_{XH}	1.1400	1.1219	1.1203	1.5242	1.6028	1.7901
$XH(A^4\Sigma^-)$	R_{XH}	1.1066	1.0908	1.0894	1.4969	1.5694	1.7550
$XH(\alpha^2\Delta)$	R_{XH}	1.1229	1.1069	1.1056			
$XH_2(^3B_1)$	R_{XH}	1.0943	1.0791	1.0775	1.4815	1.5449	1.7281
	φ_{HXH}	66.53	66.78	66.81	59.19	59.70	59.31
$XH_2(^1A_1)$	R_{XH}	1.1271	1.1107	1.1088	1.5184	1.5963	1.7841
	φ_{HXH}	50.57	50.94	51.00	46.14	45.82	45.60
$XH_3(X^2A_1)$	R_{XH}	1.0932	1.0795	1.0780	1.4810	1.5443	1.7289
	φ_{HXH}	120.00	120.00	120.00	107.59	107.68	109.21
$XH_4(X^1A_1)$	R_{XH}	1.1027	1.0899	1.0883	1.4803	1.5414	1.7289
	φ_{HXH}	109.47	109.47	109.47	109.49	109.47	109.21

the largest one in the MBE and the rest of the terms oscillating in sign and diminishing after that. The behavior of the MBE is similar across the series. The correlation between the X–H distances and the magnitude of the individual 2-B_{XH} terms, discussed earlier, is shown in Fig. 14 for the XH_n series. The linear correlation across the XH_n series for each n confirms that the X–H distance is a descriptor of the magnitude of the individual 2-B_{XH} terms. Note the difference in the magnitude of the 2-B terms for the XH series due to the absence of a 1-B term for this case. This is because the individual 2-B terms are determined with respect to the $C(^3P)$ + $H(^2S)$ for XH and with respect to the $C(^5S)$ + n × $H(^2S)$ for the XH_n, n = 2, 3, 4 series. It is interesting that this descriptor is independent of n, i.e., the size of the XH_n molecules. The linear fits corresponding to the same *in situ* atoms are almost identical as shown in Fig. 14

The variation of the individual 2-B_{HH} and 2-B_{XH} terms for the XH_n series, X = C, Si, Ge, Se and n = 2–4 is shown in Fig. 15. In the left panel, which shows the variation of the 2-B_{HH} across the series, the filled symbols trace states in which X is at the *in situ* ^5S atomic state, whereas the open symbols denote states in which X is at the *in situ* ^3P atomic state. The larger relative increase in the 2-B_{HH} term across the CH_n series is due to the fact that the hydrogen atoms are closer to one another with increasing n as the result of the shorter C–H distances being in the 1.08–1.12 Å range (cf. Table V). In contrast, the 2-B_{HH} terms for XH_n, where X = Si, Ge, and Sn, are almost the same for n = 2–4, a result of the longer X–H distances (1.50 –1.80 Å range, cf. Table V) that bring the hydrogen atoms further apart. The variation of the 2-B_{XH} term across the series is shown on the right panel of Fig. 15, where the two different curves refer to the calculation when the heavy atom is at the *in situ* ^5S and ^3P atomic states in the molecule. As a general trend, when X is at the atomic ^3P state in the molecule, we observe a monotonic decrease of the 2-B_{XH} term with the size of the X atom. This is consistent with the fact that the X–H bond distance, already being identified as a descriptor of the 2-B_{XH} term (cf. Fig. 14), increases across the series. When X is at the *in situ* atomic ^5S state, the 2-B_{XH} is also decreasing across the series, except for Ge. This "anomaly" is attributed to the fact that the $^3P \rightarrow {}^5S$ energy is the largest one for Ge (cf. Tables I–IV). It is 6.1% larger than C, 12.5% larger than Si, and 8.2% larger than Sn, resulting in the 2-$B_{Ge\text{-}H}$ term of $Ge(^5S)$ to be further stabilized.

B. Incremental bond energies: is there a "first row anomaly?"

The incremental $H_{n-1}X$–H bond energies for X = C, Si, Ge, Sn are shown in Fig. 16. In the left panel of that figure, the energies are computed *with respect to the lowest in energy* (ground states) of the $H_{n-1}X$ molecule. Following our previous discussion in Sec. III A, these are $^3B_1$ for CH_2 and $^1A_1$ for SiH_2, GeH_2, and SnH_2 (indicated

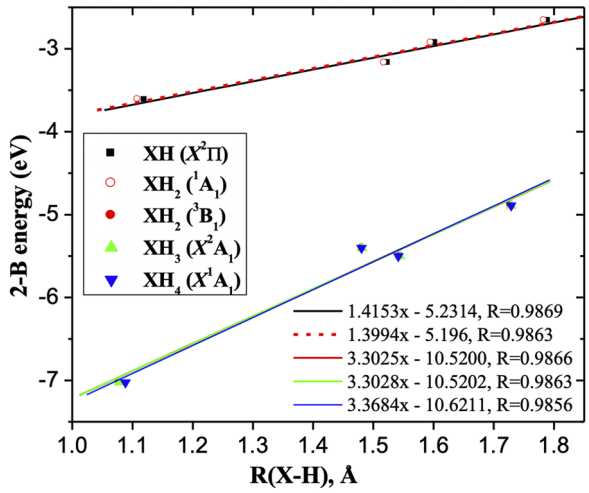

FIG. 14. Correlation between the individual 2-B_{XH} term and the X–H distance for the XH_n series, X = C, Si, Ge, Se and n = 1–4. Note the different magnitude for the XH species due to the fact that the energy difference is taken with respect to the ground state atoms (consistent with the absence of the 1-B term) for that case.

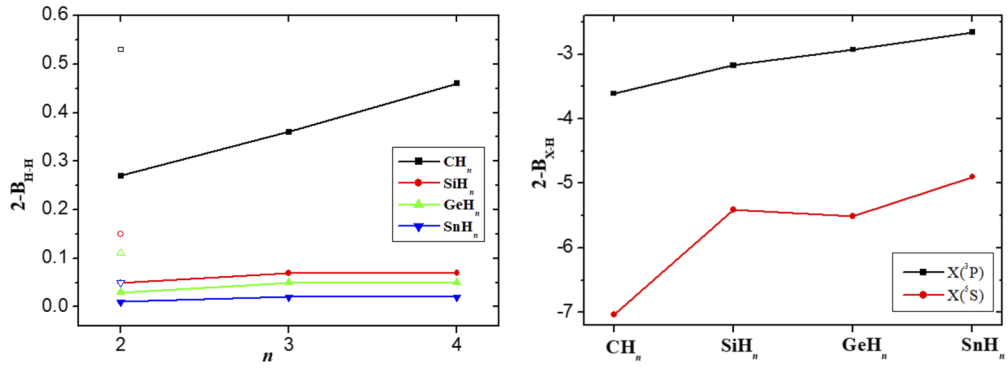

FIG. 15. Variation of the individual 2-B_{HH} and 2-B_{XH} terms for the XH_n series, X = C, Si, Ge, Se and n = 2–4 at the RCCSD(T)/AVQZ(-PP)$_{Sn}$ level of theory. In the left panel, solid/open symbols denote the states in which X is at the $^5S/^3P$ atomic states.

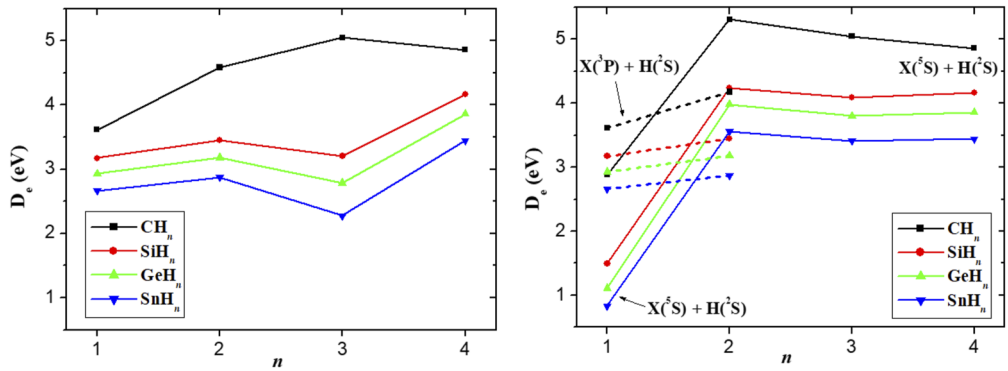

FIG. 16. The incremental $H_{n-1}X$–H bond energy, X = C, Si, Ge, Sn. Left panel: energies with respect to the lowest in energy of the $H_{n-1}X$ molecule. Right panel: energies with respect to the $H_{n-1}X$ molecule, where X is at the ^5S state (solid line) and at the ^3P state (dotted line). All energies are computed at the RCCSD(T)/AVQZ(-PP)$_{Sn}$ level of theory.

on the left panel of Fig. 16 for n = 2). The left panel of Fig. 16 is the same as the right panel of Fig. 9 of Ref. 76, but extended for X = Sn. As discussed in this earlier publication and reproduced by our results, the trend in the incremental bond energies with respect to the lowest in energy states is qualitatively different between the CH_n and the rest of XH_n series: indeed, there exists a "peak" for CH_3 (the bond energy for CH_3 is larger than the ones for CH_2 and CH_5), whereas there is a "dip" for the XH_n, X = Si, Ge, Sn, series (the bond energy for XH3 is lower than that for XH_2 and XH_5 when X = Si, Ge, Sn).

However, when the bond energies are computed *with respect to the molecular states having the same in situ atomic state* (i.e., not necessarily the lowest energy ones but the ones correlating with the same atomic states), the situation is different as shown in the right panel of Fig. 16. In that panel, the various states, with respect to which the individual incremental energies were computed, are noted. The $H_{n-1}X$–H incremental bond energies are obtained with respect to the $H_{n-1}X$ molecule, where X is at either the ^5S (solid line) or at the ^3P (dotted line) atomic states. When this protocol is followed, the variation of the bond energies with n is qualitatively similar across the series and the concept of the "first row anomaly" is not justified. One can nevertheless argue that the (first row) carbon atom can be still considered different than the (second and subsequent rows) Si, Ge, and Sn atoms *in lieu* of the "flipping" of the ground/excited states for n = 2 in the series (CH_2 vs $SiH_2/GeH_2/SnH_2$). However, this qualitative change is not a property of the individual atoms *per se* but rather their different behavior in just the XH_2, but not the rest of the hydrides.

IV. CONCLUSIONS

We have described a novel decomposition scheme for the MBE in molecules and applied it to the XH_n series (X = C, Si, Ge, Sn; n = 1–4). The protocol allows for the decomposition of the atomization energy in terms of atoms, dimers, trimers, etc. In the present implementation of the MBE that is based on the breaking of covalent bonds to define subsystems, the 1-B term is both qualitative and quantitatively different than the analogous 1-B term that has been popularized in the MBE of aqueous ionic systems. When breaking

hydrogen bonds to define the various subsystems, the 1-B term represents the geometrical distortion[94] of the individual fragments from their gas phase geometries due to the interaction with other neighboring molecules or ions. It amounts to a few kcal/mol and it can be indirectly probed experimentally by infrared (IR) spectroscopy,[99,100] which records the change in the position of the individual vibrational bands from the gas phase as a result of the change in the fragment's geometry from the isolated species. In contrast, when breaking covalent bonds, the 1-B represents the electronic excitation of an individual atom[101] to bring it to its *in situ* electronic state in the molecule, and it amounts to a few eV (i.e., it is about two orders of magnitude larger) and can be probed by Ultraviolet–Visible (UV) spectroscopy.

We have found that the MBE in the XH_n series is oscillating between positive and negative values, and it is converging with increasing rank of the expansion. Among the individual terms, the 2-B is by far the largest one in the MBE. The X–H distance is a good descriptor of the strength of the 2-B_{XH} term, and its variation across the series can be attributed to the respective geometrical changes. The analysis can offer an alternative explanation for the purported "first row anomaly" that is based upon the different variation of the incremental bond energies for CH_n compared to XH_n, X = Si, Ge, Sn, when these bond energies are evaluated with respect to the lowest energies (ground states) of the members in the series. However, there is a "flipping" between the ground and the first excited state in CH_2 (ground is the $^3B_1$ and excited is the $^1A_1$ states) compared to XH_2, where X = Si, Ge, and Sn (ground is the $^1A_1$ and excited is the $^3B_1$ state). When these incremental binding energies are evaluated with respect to the molecular states that have the same *in situ* atomic state, their variation is the same with *n* for all X (C, Si, Ge, Sn) in the XH_n series and the concept of the "first row anomaly" is, thus, not justified.

Note that the present analysis is simplified due to the presence of just one heavy atom (C, Si, Ge, Sn) in each of the systems studied and can be much more complex when more than one heavy atom is involved. Nevertheless, it provides a straightforward extension of the popular MBE for hydrogen bonded systems to incorporate the breaking of covalent bonds and offers valuable insights into the chemical bonding of chemical systems.

ACKNOWLEDGMENTS

S.S.X. was supported from the Center for Scalable Predictive methods for Excitations and Correlated phenomena (SPEC), which is funded by the U.S. Department of Energy, Office of Science, Basic Energy Sciences, Chemical Sciences, Geosciences and Biosciences Division as part of the Computational Chemical Sciences (CCS) program at Pacific Northwest National Laboratory. Battelle operates the Pacific Northwest National Laboratory for the U.S. Department of Energy. This research used computer resources provided by the National Energy Research Scientific Computing Center, which is supported by the Office of Science of the U.S. Department of Energy under Contract No. DE-AC02-05CH11231.

AUTHOR DECLARATIONS

Conflict of Interest

The authors have no conflicts to disclose.

Author Contributions

Demeter Tzeli: Data curation (lead); Formal analysis (equal); Investigation (equal); Visualization (lead). **Sotiris S. Xantheas:** Conceptualization (lead); Funding acquisition (lead); Methodology (lead); Resources (lead); Writing – original draft (lead); Writing – review & editing (lead).

DATA AVAILABILITY

The data that support the findings of this study are available from the corresponding author upon reasonable request.

REFERENCES

[1] F. Roberts and B. Tesman, *Applied Combinatorics*, 2nd ed. (CRC Press, 2009).
[2] D. Hankins, J. W. Moskowitz, and F. H. Stillinger, Jr., J. Chem. Phys. **53**, 4544–4554 (1970).
[3] S. S. Xantheas and T. H. Dunning, "The structure of the water trimer from *ab initio* calculations," J. Chem. Phys. **98**, 8037–8040 (1993).
[4] S. S. Xantheas, "*Ab initio* studies of cyclic water clusters $(H_2O)n$, *n* = 1–6. II. Analysis of many-body interactions," J. Chem. Phys. **100**, 7523–7534 (1994).
[5] S. S. Xantheas and T. H. Dunning, "Structures and energetics of F-(H_2O)n, n = 1–3, clusters from ab initio calculations," J. Phys. Chem. **98**, 13489–13497 (1994).
[6] S. S. Xantheas, "Quantitative description of hydrogen bonding in chloride-water clusters," J. Phys. Chem. **100**, 9703–9713 (1996).
[7] S. S. Xantheas, "Significance of higher-order many-body interaction energy terms in water clusters and bulk water," Philos. Mag. B **73**, 107–115 (1996).
[8] M. P. Hodges, A. J. Stone, and S. S. Xantheas, "Contribution of many-body terms to the energy for small water clusters: A comparison of ab initio calculations and accurate model potentials," J. Phys. Chem. A **101**, 9163–9168 (1997).
[9] S. S. Xantheas, "Cooperativity and hydrogen bonding network in water clusters," Chem. Phys. **258**, 225–231 (2000).
[10] R. M. Richard and J. M. Herbert, "A generalized many-body expansion and a unified view of fragment-based methods in electronic structure theory," J. Chem. Phys. **137**, 064113 (2012).
[11] R. M. Richard and J. M. Herbert, "Many-body expansion with overlapping fragments: Analysis of two approaches," J. Chem. Theory Comput. **9**, 1408–1416 (2013).
[12] R. M. Richard, K. U. Lao, and J. M. Herbert, "Approaching the complete-basis limit with a truncated many-body expansion," J. Chem. Phys. **139**, 224102 (2013).
[13] R. M. Richard, K. U. Lao, and J. M. Herbert, "Understanding the many-body expansion for large systems. I. Precision considerations," J. Chem. Phys. **141**, 014108 (2014).
[14] K. U. Lao, K.-Y. Liu, R. M. Richard, and J. M. Herbert, "Understanding the many-body expansion for large systems. II. Accuracy considerations," J. Chem. Phys. **144**, 164105 (2016).
[15] J. Liu and J. M. Herbert, "Pair–pair approximation to the generalized many-body expansion: An alternative to the four-body expansion for ab initio prediction of protein energetics via molecular fragmentation," J. Chem. Theory Comput. **12**, 572–584 (2016).
[16] K.-Y. Liu and J. M. Herbert, "Understanding the many-body expansion for large systems. III. Critical role of four-body terms, counterpoise corrections, and cutoffs," J. Chem. Phys. **147**, 161729 (2017).
[17] K.-Y. Liu and J. M. Herbert, "Energy-screened many-body expansion: A practical yet accurate fragmentation method for quantum chemistry," J. Chem. Theory Comput. **16**, 475–487 (2020).
[18] R. A. Christie and K. D. Jordan, in *Intermolecular Forces and Clusters II. Structure and Bonding*, edited by D. J. Wales (Springer, 2005), Vol. 116, pp. 27–41.
[19] E. E. Dahlke and D. G. Truhlar, "Electrostatically embedded many-body expansion for simulations," J. Chem. Theory Comput. **4**, 1–6 (2008).
[20] J. F. Ouyang, M. W. Cvitkovic, and R. P. A. Bettens, "Trouble with the many-body expansion," J. Chem. Theory Comput. **10**, 3699–3707 (2014).

[21] S. Prasad, J. Lee, and M. Head-Gordon, "Polarized many-body expansion: A perfect marriage between embedded mean-field theory and variational many-body expansion," in *Abstracts of Papers of the American Chemical Society* (American Chemical Society, 2019), Vol. 257.
[22] M. A. Collins, M. W. Cvitkovic, and R. P. A. Bettens, "The combined fragmentation and systematic molecular fragmentation methods," Acc. Chem. Res. **47**, 2776–2785 (2014).
[23] M. A. Collins and R. P. A. Bettens, "Energy-based molecular fragmentation methods," Chem. Rev. **115**, 5607–5642 (2015).
[24] R. M. Richard, K. U. Lao, and J. M. Herbert, "Aiming for benchmark accuracy with the many-body expansion," Acc. Chem. Res. **47**, 2828–2836 (2014).
[25] W. Chen and M. S. Gordon, "Energy decomposition analyses for many-body interaction and applications to water complexes," J. Phys. Chem. **100**, 14316–14328 (1996).
[26] M. S. Gordon *et al.*, "Accurate methods for large molecular systems," J. Phys. Chem. B **113**, 9646–9663 (2009).
[27] M. S. Gordon, D. G. Fedorov, S. R. Pruitt, and L. V. Slipchenko, "Fragmentation methods: A route to accurate calculations on large systems," Chem. Rev. **112**, 632–672 (2012).
[28] J. P. Heindel and S. S. Xantheas, "The many-body expansion for aqueous systems revisited: I. Water–water interactions," J. Chem. Theory Comput. **16**, 6843–6855 (2020).
[29] J. P. Heindel and S. S. Xantheas, "The many-body expansion for aqueous systems revisited: II. Alkali metal and halide ion–water interactions," J. Chem. Theory Comput. **17**, 2200–2216 (2021).
[30] K. M. Herman, J. P. Heindel, and S. S. Xantheas, "The many-body expansion for aqueous systems revisited: III. Hofmeister ion–water interactions," Phys. Chem. Chem. Phys. **23**, 11196–11210 (2021).
[31] J. P. Heindel and S. S. Xantheas, "Molecular dynamics driven by the many-body expansion (MBE-MD)," J. Chem. Theory Comput. **17**, 7341–7352 (2021).
[32] C. J. Burnham, J. Li, S. S. Xantheas, and M. Leslie, "The parametrization of a Thole-type all-atom polarizable water model from first principles and its application to the study of water clusters (n = 2–21) and the phonon spectrum of ice Ih," J. Chem. Phys. **110**, 4566–4581 (1999).
[33] .S. S. Xantheas, C. J. Burnham, and R. J. Harrison, "Development of transferable interaction models for water. II. Accurate energetics of the first few water clusters from first principles," J. Chem. Phys. **116**, 1493–1499 (2002).
[34] C. J. Burnham and S. S. Xantheas, "Development of transferable interaction models for water. III. Reparametrization of an all-atom polarizable rigid model (TTM2-R) from first principles," J. Chem. Phys. **116**, 1500–1510 (2002).
[35] C. J. Burnham and S. S. Xantheas, "Development of transferable interaction models for water. IV. A flexible, all-atom polarizable potential (TTM2-F) based on geometry dependent charges derived from an *ab initio* monomer dipole moment surface," J. Chem. Phys. **116**, 5115–5124 (2002).
[36] G. S. Fanourgakis and S. S. Xantheas, "The flexible, polarizable, thole-type interaction potential for water (TTM2-F) revisited," J. Phys. Chem. A **110**, 4100–4106 (2006).
[37] G. S. Fanourgakis and S. S. Xantheas, "The bend angle of water in ice Ih and liquid water: The significance of implementing the nonlinear monomer dipole moment surface in classical interaction potentials," J. Chem. Phys. **124**, 174504 (2006).
[38] G. S. Fanourgakis and S. S. Xantheas, "Development of transferable interaction potentials for water. V. Extension of the flexible, polarizable, Thole-type model potential (TTM3-F, v. 3.0) to describe the vibrational spectra of water clusters and liquid water," J. Chem. Phys. **128**, 074506 (2008).
[39] G. S. Fanourgakis, G. K. Schenter, and S. S. Xantheas, "A quantitative account of quantum effects in liquid water," J. Chem. Phys. **125**, 141102 (2006).
[40] V. Babin, C. Leforestier, and F. Paesani, "Development of a 'first principles' water potential with flexible monomers: Dimer potential energy surface, VRT spectrum, and second virial coefficient," J. Chem. Theory Comput. **9**, 5395–5403 (2013).
[41] V. Babin, G. R. Medders, and F. Paesani, "Development of a 'first principles' water potential with flexible monomers. II: Trimer potential energy surface, third virial coefficient, and small clusters," J. Chem. Theory Comput. **10**, 1599–1607 (2014).
[42] G. R. Medders, V. Babin, and F. Paesani, "Development of a 'first-principles' water potential with flexible monomers. III. Liquid phase properties," J. Chem. Theory Comput. **10**, 2906–2910 (2014).
[43] G. R. Medders, A. W. Götz, M. A. Morales, P. Bajaj, and F. Paesani, "On the representation of many-body interactions in water," J. Chem. Phys. **143**, 104102 (2015).
[44] D. J. Arismendi-Arrieta, M. Riera, P. Bajaj, R. Prosmiti, and F. Paesani, "i-TTM model for ab initio-based ion–water interaction potentials. 1. Halide–water potential energy functions," J. Phys. Chem. B **120**, 1822–1832 (2016).
[45] S. K. Reddy *et al.*, "On the accuracy of the MB-pol many-body potential for water: Interaction energies, vibrational frequencies, and classical thermodynamic and dynamical properties from clusters to liquid water and ice," J. Chem. Phys. **145**, 194504 (2016).
[46] M. Riera, A. W. Götz, and F. Paesani, "The i-TTM model for *ab initio*-based ion–water interaction potentials. II. Alkali metal ion–water potential energy functions," Phys. Chem. Chem. Phys. **18**, 30334–30343 (2016).
[47] Y. Wang and J. M. Bowman, "Towards an *ab initio* flexible potential for water, and post-harmonic quantum vibrational analysis of water clusters," Chem. Phys. Lett. **491**, 1–10 (2010).
[48] Y. Wang and J. M. Bowman, "*Ab initio* potential and dipole moment surfaces for water. II. Local-monomer calculations of the infrared spectra of water clusters," J. Chem. Phys. **134**, 154510 (2011).
[49] Y. Wang, X. Huang, B. C. Shepler, B. J. Braams, and J. M. Bowman, "Flexible, *ab initio* potential, and dipole moment surfaces for water. I. Tests and applications for clusters up to the 22-mer," J. Chem. Phys. **134**, 094509 (2011).
[50] R. Conte, C. Qu, and J. M. Bowman, "Permutationally invariant fitting of many-body, non-covalent interactions with application to three-body methane–water–water," J. Chem. Theory Comput. **11**, 1631–1638 (2015).
[51] A. K. Samanta, Y. Wang, J. S. Mancini, J. M. Bowman, and H. Reisler, "Energetics and predissociation dynamics of small water, HCl, and mixed HCl-water clusters," Chem. Rev. **116**, 4913–4936 (2016).
[52] R. Schwan *et al.*, "Observation of the low-frequency spectrum of the water trimer as a sensitive test of the water-trimer potential and the dipole-moment surface," Angew. Chem., Int. Ed. **59**, 11399–11407 (2020).
[53] A. Nandi *et al.*, "A CCSD(T)-based 4-body potential for water," J. Phys. Chem. Lett. **12**, 10318–10324 (2021).
[54] S. R. Gadre, R. N. Shirsat, and A. C. Limaye, "Molecular tailoring approach for simulation of electrostatic properties," J. Phys. Chem. **98**, 9165–9169 (1994).
[55] S. D. Yeole and S. R. Gadre, "Molecular cluster building algorithm: Electrostatic guidelines and molecular tailoring approach," J. Chem. Phys. **134**, 084111 (2011).
[56] N. Sahu, S. D. Yeole, and S. R. Gadre, "Appraisal of molecular tailoring approach for large clusters," J. Chem. Phys. **138**, 104101 (2013).
[57] N. Sahu and S. R. Gadre, "Molecular tailoring approach: A route for *ab initio* treatment of large clusters," Acc. Chem. Res. **47**, 2739–2747 (2014).
[58] M. M. Deshmukh and S. R. Gadre, "Molecular tailoring approach for the estimation of intramolecular hydrogen bond energy," Molecules **26**, 2928 (2021).
[59] N. Sahu *et al.*, "Low energy isomers of $(H_2O)_{25}$ from a hierarchical method based on Monte Carlo temperature basin paving and molecular tailoring approaches benchmarked by MP2 calculations," J. Chem. Phys. **141**, 164304 (2014).
[60] J. Liu and X. He, "Fragment-based quantum mechanical approach to biomolecules, molecular clusters, molecular crystals and liquids," Phys. Chem. Chem. Phys. **22**, 12341–12367 (2020).
[61] Z. Wang, Y. Han, J. Li, and X. He, "Combining the fragmentation approach and neural network potential energy surfaces of fragments for accurate calculation of protein energy," J. Phys. Chem. B **124**, 3027–3035 (2020).
[62] C. Shen, X. Jin, W. J. Glover, and X. He, "Accurate prediction of absorption spectral shifts of proteorhodopsin using a fragment-based quantum mechanical method," Molecules **26**, 4486 (2021).
[63] S. Hirata *et al.*, "Fast electron correlation methods for molecular clusters in the ground and excited states," Mol. Phys. **103**, 2255–2265 (2005).
[64] X. He, O. Sode, S. S. Xantheas, and S. Hirata, "Second-order many-body perturbation study of ice Ih," J. Chem. Phys. **137**, 204505 (2012).

[65]J. S. Boschen, D. Theis, K. Ruedenberg, and T. L. Windus, "Accurate ab initio potential energy curves and spectroscopic properties of the four lowest singlet states of C_2," Theor. Chem. Acc. **133**, 1425 (2013).
[66]J. S. Boschen, D. Theis, K. Ruedenberg, and T. L. Windus, "Correlation energy extrapolation by many-body expansion," J. Phys. Chem. A **121**, 836–844 (2017).
[67]L. Bytautas and K. Ruedenberg, "Correlation energy extrapolation by intrinsic scaling. III. Compact wave functions," J. Chem. Phys. **121**, 10852–10862 (2004).
[68]L. Bytautas and K. Ruedenberg, "Correlation energy extrapolation by intrinsic scaling. I. Method and application to the neon atom," J. Chem. Phys. **121**, 10905–10918 (2004).
[69]L. Bytautas and K. Ruedenberg, "Correlation energy extrapolation by intrinsic scaling. II. The water and the nitrogen molecule," J. Chem. Phys. **121**, 10919–10934 (2004).
[70]L. Bytautas and K. Ruedenberg, "Correlation energy extrapolation by intrinsic scaling. IV. Accurate binding energies of the homonuclear diatomic molecules carbon, nitrogen, oxygen and fluorine," J. Chem. Phys. **122**, 154110 (2005).
[71]L. Bytautas and K. Ruedenberg, "Correlation energy extrapolation by intrinsic scaling. V. Electronic energy, atomization energy, and enthalpy of formation of water," J. Chem. Phys. **124**, 174304 (2006).
[72]L. Bytautas and K. Ruedenberg, "Accurate *ab initio* potential energy curve of O_2. I. Nonrelativistic full configuration interaction valence correlation by the correlation energy extrapolation by intrinsic scaling method," J. Chem. Phys. **132**, 074109 (2010).
[73]H. Stoll, "Correlation-energy of diamond," Phys. Rev. B **46**, 6700–6704 (1992).
[74]H. Stoll, B. Paulus, and P. Fulde, "On the accuracy of correlation-energy expansions in terms of local increments," J. Chem. Phys. **123**, 144108 (2005).
[75]B. Paulus, "The method of increments—A wavefunction-based ab initio correlation method for solids," Phys. Rep. **428**, 1–52 (2006).
[76]L. T. Xu, J. V. K. Thompson, and T. H. Dunning, "Spin-coupled generalized valence bond description of group 14 species: The carbon, silicon and germanium hydrides, XH_n (n = 1–4)," J. Phys. Chem. A **123**, 2401–2419 (2019).
[77]G. L. Miessler and D. A. Tarr, *Inorganic Chemistry*, 3rd ed. (Pearson Prentice Hall, 1991).
[78]W. Kutzelnigg, "Chemical bonding in higher main group elements," Angew. Chem., Int. Ed. **23**, 272–295 (1984).
[79]W. Heitler, "Quantum chemistry: The early period," Int. J. Quantum Chem. **1**, 13–36 (1967).
[80]N. Takeda *et al.*, "Gas phase protonated nicotine is a mixture of pyridine- and pyrrolidine-protonated conformers: Implications for its native structure in the nicotinic acetylcholine receptor," Phys. Chem. Chem. Phys. **24**, 5786–5793 (2022).
[81]A. Kalemos and A. Mavridis, "Bonding elucidation of the three common acids H_2SO_4, HNO_3, and $HClO_4$," J. Phys. Chem. A **113**, 13972–13975 (2009).
[82]A. Kalemos, I. R. Ariyarathna, S. N. Khan, E. Miliordos, and A. Mavridis, "'Hypervalency' and the chemical bond," Comput. Theor. Chem. **1153**, 65–74 (2019).
[83]E. Miliordos and S. S. Xantheas, "Ground and excited states of the $[Fe(H_2O)_6]^{2+}$ and $[Fe(H_2O)_6]^{3+}$ clusters: Insight into the electronic structure of the $[Fe(H_2O)_6]^{2+}$–$[Fe(H_2O)_6]^{3+}$ complex," J. Chem. Theory Comput. **11**, 1549–1563 (2015).
[84]E. Miliordos and S. S. Xantheas, "Elucidating the mechanism behind the stabilization of multi-charged metal cations in water: A case study of the electronic states of microhydrated Mg^{2+}, Ca^{2+} and Al^{3+}," Phys. Chem. Chem. Phys. **16**, 6886–6892 (2014).
[85]G. D. Purvis and R. J. Bartlett, "A full coupled-cluster singles and doubles model: The inclusion of disconnected triples," J. Chem. Phys. **76**, 1910–1918 (1982).
[86]M. J. O. Deegan and P. J. Knowles, "Perturbative corrections to account for triple excitations in closed and open-shell coupled-cluster theories," Chem. Phys. Lett. **227**, 321–326 (1994).
[87]T. H. Dunning, "Gaussian-basis sets for use in correlated molecular calculations .I. The atoms boron through neon and hydrogen," J. Chem. Phys. **90**, 1007–1023 (1989).
[88]R. A. Kendall, T. H. Dunning, and R. J. Harrison, "Electron-affinities of the first-row atoms revisited. Systematic basis-sets and wave-functions," J. Chem. Phys. **96**, 6796–6806 (1992).
[89]D. E. Woon and T. H. Dunning, "Gaussian-basis sets for use in correlated molecular calculations. III. The atoms aluminum through argon," J. Chem. Phys. **98**, 1358–1371 (1993).
[90]A. K. Wilson, D. E. Woon, K. A. Peterson, and T. H. Dunning, "Gaussian basis sets for use in correlated molecular calculations. IX. The atoms gallium through krypton," J. Chem. Phys. **110**, 7667–7676 (1999).
[91]K. A. Peterson, "Systematically convergent basis sets with relativistic pseudopotentials. I. Correlation consistent basis sets for the post-*d* group 13–15 elements," J. Chem. Phys. **119**, 11099–11112 (2003).
[92]S. F. Boys and F. Bernardi, "Calculation of small molecular interactions by differences of separate total energies. Some procedures with reduced errors," Mol. Phys. **19**, 553–566 (1970).
[93]B. Liu and A. D. McLean, "Accurate calculation of attractive interaction of two ground-state helium-atoms," J. Chem. Phys. **59**, 4557–4558 (1973).
[94]S. S. Xantheas, "On the importance of the fragment relaxation energy terms in the estimation of the basis set superposition error correction to the intermolecular interaction energy," J. Chem. Phys. **104**, 8821–8824 (1996).
[95]I. N. Levine, *Quantum Chemistry* (Prentice Hall, 1991).
[96]T. J. Lee and P. R. Taylor, "A diagnostic for determining the quality of single-reference electron correlation methods," Int. J. Quantum Chem. **36**, 199–207 (1989).
[97]T. J. Lee, J. E. Rice, G. E. Scuseria, and H. F. Schaefer, "Theoretical investigations of molecules composed only of fluorine, oxygen and nitrogen: determination of the equilibrium structures of FOOF, $(NO)_2$ and FNNF and the transition-state structure for FNNF *cis-trans* isomerization," Theor. Chim. Acta **75**, 81–98 (1989).
[98]H.-J. Werner, P. J. Knowles, G. Knizia, F. R. Manby, and M. Schütz, "Molpro: a general-purpose quantum chemistry program package," Wiley Interdisciplinary Rev. Comput. Mol. Sci. **2**, 242–253 (2012).
[99]J. A. Fournier *et al.*, "Snapshots of proton accommodation at a microscopic water surface: Understanding the vibrational spectral signatures of the charge defect in cryogenically cooled $H^+(H_2O)_{n=2-28}$ clusters," J. Phys. Chem. A **119**, 9425–9440 (2015).
[100]N. Yang *et al.*, "Mapping the temperature-dependent and network site-specific onset of spectral diffusion at the surface of a water cluster cage," Proc. Natl. Acad. Sci. U. S. A. **117**, 26047–26052 (2020).
[101]C. E. Moore, *National Standard Reference Data Series* (US National Bureau of Standards, Office of Standard Reference Data, Washington DC, 1972), Vols. I–III.